Table 1 Angle included between satellite polar axis and the local vertical: Satellite 1963 22A, June 22, 1963

Universal time			Along orbit, deg	Across orbit, deg
hr	min	sec		
11	58	53	7.0	−19.1
	59	15	6.3	−18.7
12	00	21	2.5	−16.9
	00	43	4.6	−17.5
	01	49	2.1	−15.6
	02	11	1.5	−14.5
	03	39	2.4	−13.0
	04	01	1.1	−11.9
	07	20	−1.5	− 5.6
	07	42	−1.7	− 5.4
	08	48	−2.2	− 2.9
	09	10	−2.5	− 1.9

and **b** are linearly independent, we obviously have the relationship

$$\begin{pmatrix}(\mathbf{R}\times\mathbf{B})_1\\(\mathbf{R}\times\mathbf{B})_2\\(\mathbf{R}\times\mathbf{B})_3\end{pmatrix} = \{A\}\begin{pmatrix}(\mathbf{r}\times\mathbf{b})_1\\(\mathbf{r}\times\mathbf{b})_2\\(\mathbf{r}\times\mathbf{b})_3\end{pmatrix} \tag{3}$$

Equations (1–3) are then combined into a single equation:

$$\left\{\begin{matrix}R_1 & B_1 & (\mathbf{R}\times\mathbf{B})_1\\R_2 & B_2 & (\mathbf{R}\times\mathbf{B})_2\\R_3 & B_3 & (\mathbf{R}\times\mathbf{B})_3\end{matrix}\right\} = \{A\}\left\{\begin{matrix}r_1 & b_1 & (\mathbf{r}\times\mathbf{b})_1\\r_2 & b_2 & (\mathbf{r}\times\mathbf{b})_2\\r_3 & b_3 & (\mathbf{r}\times\mathbf{b})_3\end{matrix}\right\} \tag{4}$$

As the matrix on the extreme right of Eq. (4) has columns that are the components of linearly independent vectors, its inverse necessarily exists. Thus, by inverting this matrix, we can solve for the attitude matrix, $\{A\}$.† A simple extension facilitates this inversion: If we use for the third column (rather than the components of $\mathbf{r} \times \mathbf{b}$) the components of $\mathbf{r} \times \mathbf{b}/|\mathbf{r} \times \mathbf{b}|$, and for the first column the components of $\mathbf{b} \times (\mathbf{r} \times \mathbf{b}/|\mathbf{r} \times \mathbf{b}|)$, then the matrix we have to invert is an orthogonal matrix that can be inverted at sight.‡ These details, however, are only of computational interest, as Eq. (4) embodies the crucial idea necessary to obtain the solution.

Once the attitude matrix is obtained, it is a trivial matter to obtain the orientation of the satellite relative to other known coordinate systems. A particularly convenient one that we have used is a coordinate system based on the position and angular momentum vectors of the satellite. Using this coordinate system, we compute the angle that the satellite polar axis forms with the position vector to the center of the earth. Subsequently, we resolve this angle into components along and orthogonal to the orbit plane.

Seemingly convenient for dynamic analyses would be a formal transformation of the $\{A\}$ matrix to Eulerian angles. On the other hand, the work of Marguiles and Goodman[3] has given us "pause for concern."

III. Some Results

The technique described previously was successfully used aboard the 1963 22A satellite. This satellite contained a pioneering experiment to evaluate gravity-gradient stabilization.[4] Sample results obtained are contained in Table 1. These results confirmed that the gravity stabilization system was successful.

IV. Discussion

It is clear that measurements of any two linearly independent vectors in satellite coordinates are sufficient to determine the orientation if these vectors have a known resolution in the reference coordinate system. Usually, the necessary conditions, because of available constraints, are less stringent. In our system, we chose to measure all six quantities and use three available constraints, e.g.,

$$\sum_{i=1}^{3} r_i^2 = \sum_{i=1}^{3} b_i^2 = 1 \qquad \mathbf{r}\cdot\mathbf{b} = \mathbf{R}\cdot\mathbf{B}$$

to minimize the effects of noise in the data. A discussion of this noise analysis would take us outside the scope of this paper.

References

[1] Fischell, R. E., "Solar cell experiments on the transit and TRAAC satellites (unclassified)," Johns Hopkins Univ., Applied Physics Lab. Rept. CM-1021 (May 1962).

[2] Jensen, D. C. and Cain, J. C., "An interim geomagnetic field," J. Geophys. Res. **67**, 3568 (1962).

[3] Marguiles, G. and Goodman, G. S., "Dynamical equations for the attitude matrix of an orbiting satellite," ARS J. **32**, 1414 (1962).

[4] Fischell, R. E., "Passive gravity-gradient stabilization for earth satellites," *Torques and Attitude Sensing*, edited by S. F. Singer (Academic Press Inc., New York, to be published).

---

† The writer is indebted to his colleague, Stuart Haywood of APL/JHU for pointing out this method of solving Eqs. (1) and (2).

‡ The left side of Eq. (4) is, of course, replaced with the corresponding quantities in **R** and **B**.

Buckling of Circular Cylindrical Shells in Axial Compression

R. C. Tennyson*
University of Toronto, Toronto, Ontario, Canada

Nomenclature

X, Y = mx/L, $ny/2\pi R$
l_x = L/m
m, n = number of half-waves in the axial and circumferential directions, respectively
x, y, z = reference set of orthogonal coordinate axes
u, v, w = displacements in the x, y, and z directions, respectively
L = shell length
R = initial shell radius
t = shell wall thickness
A, B, C = displacement amplitudes
σ = normal stress
τ = shear stress
ϵ = normal strain
γ = shear strain
θ = angle measured from x axis counterclockwise

RECENT tests on five circular cylindrical shells having clamped ends subjected to axial compression have yielded buckling loads within 10% of the classical predicted values.[1] All shells were made from a photoelastic plastic and behaved completely elastically, thus permitting repeatable tests. During the course of photoelastically analyzing the shells,[2] high-speed photographs of the buckling process taken through a plane reflection-type polariscope were obtained with a Fastax camera. The change in isoclinic patterns with change in buckle waveshape was recorded as a function of time. Of particular interest is the change in the 45° isoclinic during buckling for a shell with a reflective surface at some intermediate position in the shell's wall (Fig. 1). The following note describes a brief analysis of the initial stages of buckling and compares the classical waveshape with that observed in frames 3 to 6 of Fig. 1.

From the theory of photoelasticity,[3] it is known that an isoclinic of parameter θ defines the locus of points in a stressed

---

Received March 16, 1964; revision received April 10, 1964.

* Research Assistant, Institute for Aerospace Studies. Student Member AIAA.

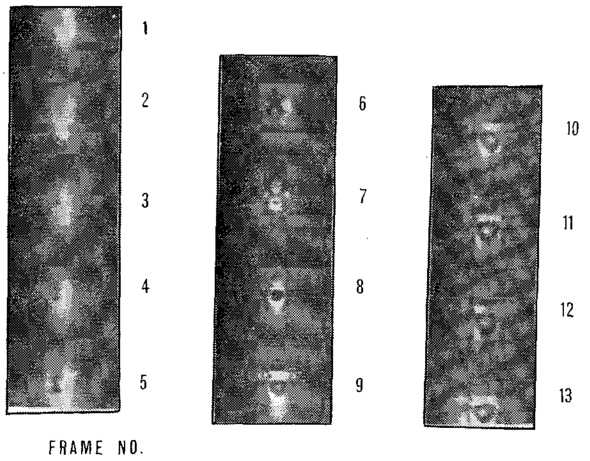

Fig. 1 The buckling process (2000 frames/sec) as viewed through a plane reflection-type polariscope set at 45°. Reflective face near midsurface in the shell's wall. Frame 3 is the start of the buckling process, and frame 12 is the final form of 45° isoclinic (buckling time = 0.005 sec).

body whose principal stresses σ_1, σ_2 are inclined at the angle θ to a set of orthogonal coordinate axes (x, y). It is also known from the theory of elasticity[4] that principal planes are shearless planes. By making use of the zero shear stress condition and the property of isoclinics, the classical buckling mode shapes can be used to derive the 45° isoclinics, which may be compared with Fig. 1, frames 3 to 6.

For a plane stress system acting on an element of shell, the shear stress on any set of rectangular axes (x', y') referred to the x-y axes can be written as

$$\tau x'y' = [(\sigma y - \sigma x)/2] \sin 2\theta + \tau xy \cos 2\theta \tag{1}$$

It is possible to choose a set of axes so that $\tau x'y' = 0$. From (1), for $\tau x'y' = 0$, the condition on angle θ is

$$\begin{aligned} \tan 2\theta &= 2\tau xy/(\sigma x - \sigma y) \\ &= \gamma_{xy}/(\epsilon_x + \epsilon_y) \qquad \text{(in terms of the strains)} \end{aligned} \tag{2}$$

Thus, for any angle θ given by (2), there will be no shearing stress but only normal stresses acting on the element. These stresses are called principal normal stresses, and the planes on which they act are principal planes. It may then be concluded that (2) defines an isoclinic of parameter θ.

At the inception of buckling, the displacement modes assumed in the classical theory are given by[5]

$$u = u_0 l_x X + A \cos\pi X \sin\pi Y \tag{3}$$

$$v = B \sin\pi X \cos\pi Y \tag{4}$$

$$w = C \sin\pi X \sin\pi Y - w_0 \tag{5}$$

where $(u_0 l_x X)$ represents the initial end-shortening prior to buckling. The shell is assumed to expand uniformly radially during loading $(-w_0)$, thus neglecting end-constraints.

The strains can be determined from the displacements by the following relations:[5]

$$\epsilon_x = \frac{\partial u}{\partial x} - z\frac{\partial^2 w}{\partial x^2} \tag{6}$$

$$\epsilon_y = \frac{\partial v}{\partial y} + \frac{w}{R} - z\frac{\partial^2 w}{\partial y^2} \tag{7}$$

$$\gamma_{xy} = \frac{\partial u}{\partial y} + \frac{\partial v}{\partial x} + 2z\frac{\partial^2 w}{\partial x \partial y} \tag{8}$$

where z defines the distance from the neutral surface of the shell wall to any fiber. In the case of membrane stresses only, $z = 0$. However, the shell used in Fig. 1 had a reflective surface at some intermediate position in the wall. As a result, all strains indicated by the photoelastic method include membrane and bending components.

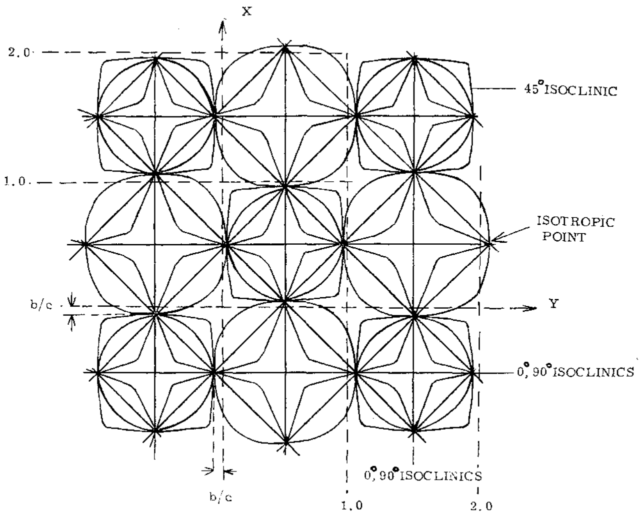

Fig. 2 Family of isoclinics [Eq. (9)] for the classical buckling mode shape.

Substituting (3–8) into (2) yields a relation of the form

$$\tan 2\theta = \frac{a \cos\pi X \cos\pi Y}{b + c \sin\pi X \sin\pi Y} \tag{9}$$

where a, b, and c are functions of the shell geometry and the displacement amplitudes. Equation (9) defines a family of isoclinics for the classical buckling mode shapes and is plotted in Fig. 2. Note that the isotropic points are displaced from the X-Y axes by an amount b/c, where b approaches zero for very long cylinders.

The 45° isoclinics in the neighborhood of (0, 0) and (1.0, 0) are redrawn in Fig. 3, ending at isotropic points. Because of the smallness of the buckles at the inception of buckling, the isoclinics are confined to a small region. As a result, they are somewhat diffuse, and no well-defined trajectory is visible at the beginning of buckling (frames 3 to 5). As the buckle grows, the isoclinics take on well-defined shapes (frames 6 to 13). An attempt was made in Fig. 3 to outline a probable boundary of the 45° classical isoclinic region, based on isoclinic data for the buckled shell in its large-deflection configuration.[2] The bounded area of Fig. 3 is seen to resemble the dark region bounded by the 45° isoclinics of frames 4 and 5 of Fig. 1, which occur near the inception of buckling. The diamond-shaped patterns visible in frames 6 to 13 occur for a buckled configuration more developed than the classical form.

High-speed photographs taken on either side of the buckled region of Fig. 1 show that the adjacent regions initially do not buckle, and buckling is localized. It was further evident that, as the buckles rapidly spread in the transverse direction, the centerline shifts (Fig. 4). Assuming that Fig. 3 depicts the initial buckling configuration, the region under observation

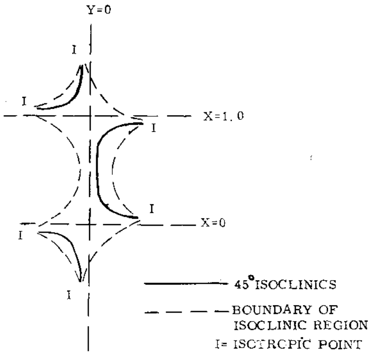

Fig. 3 45° isoclinics for the shell in its initial buckled configuration (m = 3, n = 10).

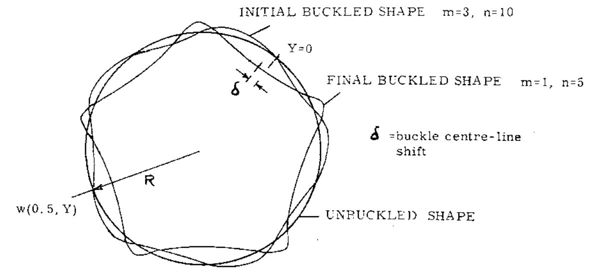

Fig. 4 End view of radial deflection pattern of shell.

can be said to have buckled into two circumferential half-waves and three axial half-waves. This particular shell in its final buckled shape developed into five large diamond-shaped buckles circumferentially, with only one axial half-wave. Since each buckle corresponds to the region photographed, it can be deduced that the shell initially buckled into 10 transverse half-waves. These results are shown in Fig. 4. For the given shell geometry, classical theory[5] predicts that $n = 10$ and $m = 12$. Disagreement occurs only in the axial wave number and can be credited to the effect of end-constraints. Theory assumes that the shell is sufficiently long so that end-conditions have negligible effect on the buckling mode.

Since theory assumes a periodic buckling pattern circumferentially and axially, it cannot be expected to yield a mode shape identical to the observed patterns at the beginning of buckling. However, it appears that the shells tested ($100 \leq R/t \leq 170, 2 \leq L/R \leq 6$) buckled elastically near the classical value with an initial wave shape approximated by the classical waveform, which rapidly degenerates into the large-deflection diamond-shaped buckles observed in the postbuckled configuration.

References

[1] Tennyson, R. C., "A note on the classical buckling load of circular cylindrical shells under axial compression," AIAA J. 1, 475–476 (1963).

[2] Annual Progr. Rept. 63-66, Institute for Aerospace Studies, Univ. of Toronto (October 1963).

[3] Frocht, M. M., *Photoelasticity* (John Wiley and Sons, Inc., New York, 1941), Vol. 1, Chap. 6.

[4] Sechler, E. E., *Elasticity in Engineering* (John Wiley and Sons, Inc., New York, 1952), Chap. 2.

[5] Timoshenko, S. P. and Gere, G. M., *Theory of Elastic Stability* (McGraw-Hill Book Co., Inc., New York, 1961), 2nd ed., Chaps. 10 and 11.

A Simple Device for the Qualitative Measurement of the Vortices

B. Lakshminarayana*
Pennsylvania State University, University Park, Pa.

Introduction

WHERE a vortex field is encountered, a qualitative assessment of the vortices would be most beneficial to the analytical treatment of the aerodynamic problem. Few attempts[1–3] have been made in this direction. Hopkins and Sorensen's[1] device consists of a cylinder, free to rotate about an axis perpendicular to the cylinder, placed in the flow field with its axis of rotation aligned in the freestream direction. The size and shape of the cylinder in combination with the bead thrust bearings used in the instrument are likely to introduce considerable error in the vorticity measurements.

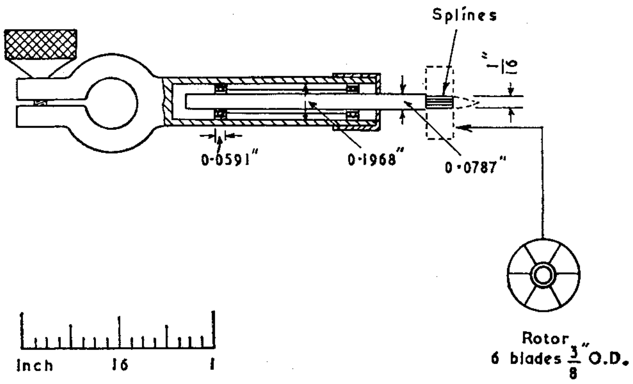

Fig. 1 Vorticity meter with miniature ball bearings.

Bobrik[2] has developed a combined pitot and vorticity meter. The latter consists of a thin plate mounted on pivots. The instrument is likely to encounter appreciable friction because of the pivoting.

Todd's[3] instrument, which has an air-floated spindle, provides very accurate results. The thickness of air cushion is 0.0005 in. This reduces the friction to almost nothing. Furthermore, there is an elaborate arrangement to measure the speed of the rotor. Remote measurements are possible from this instrument, but the manufacture and maintenance need considerable skill and care. The author's[4] experience with such an instrument was not encouraging in view of the care involved and the time consumed in taking measurements. This necessitated the design of a simple instrument (described below) without much sacrifice in sensitivity. The instrument is reliable and simple to operate.

Description of the Instrument

The instrument (Figs. 1 and 2) consists of a $\frac{5}{64}$-in.-diam spindle that runs on two miniature ball bearings. These are completely enclosed in a casing (Fig. 2) to prevent the accumulation of dust and the subsequent failure of the bearings. One end of the spindle has splines cut in it to hold the rotor in position. These rotors (Fig. 2) are filed from solid

Fig. 2 Photograph of the vorticity meter and rotors.

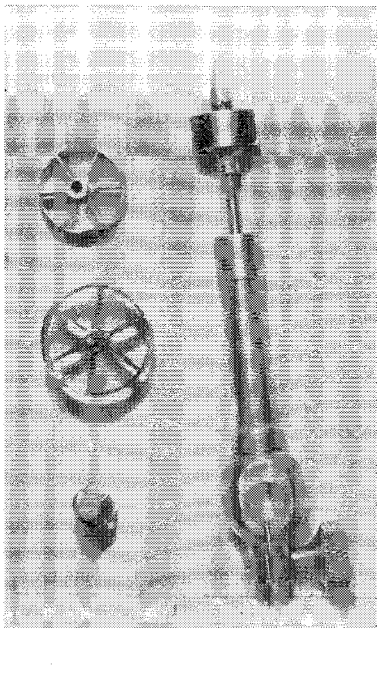

Received March 16, 1964. The instrument mentioned in this note was developed while the author was a doctoral candidate at the Liverpool University. The author wishes to thank K. W. Todd for the helpful discussions. The ingenuity and skilled craftsmanship of W. Cowie enabled the manufacture of this instrument at Liverpool University workshop.

[*] Visiting Assistant Professor, Department of Aeronautical Engineering. Member AIAA.